

Optical sensor based on resonant porous silicon structures

Jarkko J. Saarinen^{1,*}, Sharon M. Weiss², Philippe M. Fauchet^{2,3}, and J. E. Sipe¹

¹*Department of Physics, University of Toronto, 60 St. George Street, Toronto, Ontario, Canada M5S 1A7*

²*Institute of Optics, University of Rochester, P.O. Box 270186, Rochester, NY 14627-0186, United States*

³*Department of Electrical & Computer Engineering, University of Rochester, P.O. Box 270231, Rochester, NY 14627-0231, United States*

saarinen@physics.utoronto.ca

Abstract: We propose a new design for an optical sensor based on porous silicon structures. We present an analysis based on a pole expansion, which allows for the easy identification of the parameters important for the operation of the sensor, and the phenomenological inclusion of scattering losses. The predicted sensitivity of the sensor is much greater than detectors utilizing surface plasmon resonance.

© 2005 Optical Society of America

OCIS codes: (230.3990) Microstructure devices; (230.5750) Resonators; (240.6680) Surface plasmons.

References and links

1. J. Rätty, K.-E. Peiponen, and T. Asakura, *UV-visible reflection spectroscopy of liquids* (Springer, Heidelberg, 2004).
2. H. Rätther, *Surface plasmons on smooth and rough surfaces and on gratings* (Springer, Berlin, 1988).
3. E. Kretschmann, "Decay of non radiative surface plasmons into light on rough silver films. Comparison of experimental and theoretical results.," *Opt. Comm.* **6**, 185–187 (1972).
4. I. Pockrand, "Surface plasma oscillations at silver surfaces with thin transparent and absorbing coatings," *Surf. Sci.* **72**, 577–588 (1978).
5. J. D. Swalen, "Optical wave spectroscopy of molecules at surfaces," *J. Phys. Chem.* **83**, 1438–1445 (1979).
6. H. Kano and S. Kawata, "Surface-plasmon sensor for absorption-sensitivity enhancement," *Appl. Opt.* **33**, 5166–5170 (1994).
7. J. J. Saarinen, K.-E. Peiponen, and E. M. Vartiainen, "Simulation on wavelength-dependent complex refractive index of liquids obtained by phase retrieval from reflectance dip due to surface plasmon resonance," *Appl. Spectrosc.* **57**, 288–292 (2003).
8. R. J. Green, R. A. Frazier, K. M. Skakesheff, M. C. Davies, C. J. Roberts, and S. J. B. Tendler, "Surface plasmon resonance analysis of dynamic biological interactions with biomaterials," *Biomaterials* **21**, 1823–1835 (2000).
9. B. J. Sedlak, "Next-generation microarray technologies - Focus is on higher sensitivity, drug discovery, and lipid cell signaling," *Genetic Engineering News* **23**, 20–20 (2003).
10. P. M. Fauchet, "Silicon: Porous," in *Encyclopedia of applied physics, update 2*, G. L. Trigg, ed. (Wiley-VCH Verlag, New York, 1999), pp. 249–272.
11. S. M. Weiss and P. M. Fauchet, "Electrically tunable porous silicon active mirrors," *Phys. Stat. Sol. A* **197**, 556–560 (2003).
12. J. E. Lugo, J. A. del Rio, and J. Tagüieña-Martínez, "Influence of surface coverage on the effective optical properties of porous silicon modeled as a Si-wire array," *J. Appl. Phys.* **81**, 1923–1928 (1997).
13. P. E. Schmid, "Optical absorption in heavily doped silicon," *Phys. Rev. B.* **23**, 5531–5536 (1981).
14. J. von Behren, L. Tsybeskov, and P. M. Fauchet, "Preparation, properties and applications of free-standing porous silicon films," in *Microcrystalline and nanocrystalline semiconductors*, Vol. 358, R. W. Collins, C. C. Tsai, M. Hirose, F. Koch, and L. Brus, eds. (Mat. Res. Proc., 1995), pp. 333–338.
15. J. E. Sipe, "New Green-function formalism for surface optics," *J. Opt. Soc. Am. B* **4**, 481–489 (1987).

16. J. E. Sipe, "Surface plasmon-enhanced absorption of light by adsorbed molecules," *Solid State Commun.* **33**, 7–9 (1980).
17. J. E. Sipe and J. Becher, "Surface energy transfer enhanced by optical cavity excitation: a pole analysis," *J. Opt. Soc. Am.* **72**, 288–295 (1982).
18. E. D. Palik, *Handbook of optical constants of solids* (Academic Press, New York, 1985).
19. A. Yariv, *Quantum Electronics*, 3rd ed. (Wiley, New York, 1988).
20. G. Amato, L. Boarino, S. Borini, and A. M. Rossi, "Hybrid approach to porous silicon integrated waveguides," *Phys. Stat. Sol. (a)* **182**, 425–430 (2000).
21. For an overlayer thickness l with an index n_1 the effective Fresnel coefficient \tilde{r}_{51} from the prism in Fig. 1a is exactly given by Eq. (9) but with r_{31} replaced by $\hat{r}_{31} = (r_{31} + r_{11} \exp(2i\omega_1 l)) / (1 - r_{13} r_{11} \exp(2i\omega_1 l))$ in an obvious notation. Using Fresnel coefficient identities, that new equation can be written as $\hat{r}_{31} = (r_{31} + \hat{r}_{11}) / (1 + r_{31} \hat{r}_{11})$, where $\hat{r}_{11} = (r_{11} + r_{11} \exp(2i\omega_1 l)) / (1 - r_{11}^2 \exp(2i\omega_1 l))$. Using the pole approximation (11) for r_{31} in this new expression for \tilde{r}_{51} , we predict a shift of the resonance dip due to the overlayer which deviates from an exact calculation of that shift by only 0.002°.

1. Introduction

Traditionally the analysis of the complex refractive index of gases and absorbing liquids relies on measurements based on the utilization of a prism reflectometer [1]. However, there is a large improvement in the sensitivity of the system if one side of the prism is coated with a thin metal film to excite a surface plasmon resonance (SPR). Devices based on these resonances form an established optical sensing technology capable of providing accurate, sensitive, and fast detection of small changes in the refractive index of gases and liquids [2].

A typical set-up for the SPR measurements is Kretschmann's configuration [3], where one side of a high index glass prism is coated with a thin metal film, typically silver or gold (see Fig. 1a). The metal plays two roles: First, excitation through the prism sets up evanescent fields that extend to the metal-sample interface. Second, at that interface surface plasmons can be excited when the component of the incident field wave vector parallel to the surface matches the surface plasmon wave number. The reflectance is strongly decreased when this SPR condition is met, due to absorption in the metal, and the width and depth of the resonance is changed when any material is placed above the metal. Admittedly, the method is sensitive to unwanted surface defects, such as oxidation of the metal film, since the field strength is largest near the surface and the penetration depth in the sample is rather small. Nonetheless, the width of the reflectance dip and level of the reflectance minimum do yield information about the absorption of the sample [4, 5], and the accuracy of the SPR sensor can be enhanced when the thickness of the metal film is optimized [6]. In this way, SPR can be used for the retrieval of the complex refractive index of any surrounding medium [7] as well as for the detection of the molecules adsorbed to the metal film. Furthermore, by adding a thin adsorptive layer at the top of the metal film, SPR devices become very sensitive probes for the kinetics of biological binding processes [8]. In recent years SPR sensing has been employed in biological and industrial applications, and has even been used to study protein interactions in low-gravity aboard the space station [9].

In this paper we propose an alternative geometry for sensing applications, based on porous silicon (PS) structures [10] (see Fig. 1b). PS layers with a wide range of refractive indices [11] can be formed by electrochemical etching of doped silicon with hydrofluoric acid. We consider layers with pores small compared to the incident wavelength; such layers can be treated by a Maxwell Garnett type effective medium theory [12]. Our configuration of interest contains a low-index (high porosity) PS layer above the silicon substrate that provides evanescent coupling to a waveguide resonance arising due to a high index (low porosity) PS resonator layer. The coupling and resonator layers together play the role of metal film in the SPR device. The positioning of any target material to be detected in the porous layer exposes it to the full field strength of the waveguide resonance. Hence we can expect a large enhancement in the sensitivity of the PS sensor compared to the conventional SPR devices.

This paper is organized as follows: In Section 2 we first present the general formulas to calculate reflectance from the structures of interest. The pole expansions for the conventional SPR set-up and for the suggested porous silicon structure are presented in the separate subsections 2.1 and 2.2. These pole expansion expressions are then applied in Section 3, where we numerically compare the sensitivity of the conventional SPR device and our proposed resonant porous silicon structure. Our concluding remarks are given in Section 4.

2. Pole expansion analysis of the reflectance

In this paper we consider the systems presented in Fig. 1. Figure 1a represents the conventional Kretschmann's configuration, where one side of the prism is covered by a thin metal film; the light is coupled evanescently through the metal film to excite the surface plasmon at the interface between the metal and the sample. In Fig. 1b we show a porous silicon structure, where both resonance (waveguide) and coupling layer are porous silicon. The resonance layer is formed from low porosity (high refractive index) silicon to support waveguide modes, and the coupling to these modes is done from the high porosity coupling layer, where the electric field is evanescent.

In this paper we restrict ourselves to such wavelengths that absorption is small in the boron-doped silicon [13]. Small absorption allows us to couple directly through the doped silicon substrate using a high index glass prism, and thus eliminate the need to lift off thin porous silicon layers [14] from the substrate. For operation at visible wavelengths, where absorption is much increased, we would modify our configuration, employing a lift-off process to position the PS on top of non-absorbing materials. To minimize absorption losses, we could also replace the PS coupling layer by an appropriate layer of a non-absorbing low index material. We plan to turn to such structures in a later communication.

It is convenient to split the wave numbers into parallel and perpendicular pieces to the interfaces [15]. We denote wave number parallel to the surface by κ , assumed to be real. Hence, the wave number perpendicular to the surface w_i is given by

$$w_i = (\tilde{\omega}^2 \epsilon_i - \kappa^2)^{1/2} \quad (1)$$

with the vacuum wave number denoted by $\tilde{\omega} = \omega/c$ and ϵ_i is the dielectric function of the i th medium. The square root is defined such that $\text{Im}\{z^{1/2}\} \geq 0$ and $\text{Re}\{z^{1/2}\} \geq 0$, if $\text{Im}\{z^{1/2}\} = 0$. We analyze the reflectance by means of the Fresnel reflection and transmission coefficients, which in this notation are [15]

$$r_{ij}^s = \frac{w_i - w_j}{w_i + w_j} \quad ; \quad t_{ij}^s = \frac{2w_i}{w_i + w_j}, \quad (2)$$

for s-polarized light and

$$r_{ij}^p = \frac{w_i \epsilon_j - w_j \epsilon_i}{w_i \epsilon_j + w_j \epsilon_i} \quad ; \quad t_{ij}^p = \frac{2n_i n_j w_i}{w_i \epsilon_j + w_j \epsilon_i}. \quad (3)$$

for p-polarized light; the notation is that the field is incoming on an interface between media i and j from medium i . The expressions (2)–(3) are valid for absorbing medium as well, and these coefficients satisfy the Fresnel coefficient identities

$$r_{ij} = -r_{ji} \quad ; \quad t_{ij} t_{ji} - r_{ij} r_{ji} = 1. \quad (4)$$

Equations (1)–(4) are used in the derivation of the pole expansion analysis [16, 17] of the reflectance from the SPR and PS sensors in the following subsections.

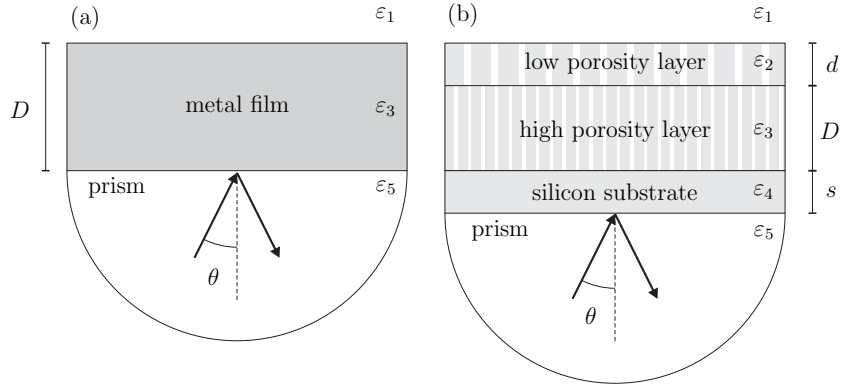


Fig. 1. Schematic diagrams of (a) Kretschmann's SPR configuration and (b) optical sensor based on porous silicon.

2.1. Pole expansion of the reflectance R_{51} from the SPR sensor

Surface plasmons are electromagnetic modes propagating at the interface between the metal film and the sample, and the phenomenon can be described as a collective oscillation of free electrons in metal layer [2]. These modes can be excited only with p-polarized light, since the incident electric field of the s-polarized light does not have a component of the wave vector parallel to the interface pointing in the direction of surface plasmon propagation along the interface. The dispersion relation for surface plasmons is obtained when the incident wave number parallel to the interface matches together with the SPR wave number. At this resonance condition the Fresnel reflection coefficient r_{31} , given by Eq. (3) for p-polarized light, diverges [16]. Hence, r_{31} has a pole at a particular wave number, and this pole signals the dispersion relation for a surface plasmon,

$$\kappa_{\text{SPR}} = \tilde{\omega} \left(\frac{\epsilon_1 \epsilon_3}{\epsilon_1 + \epsilon_3} \right)^{1/2}, \quad (5)$$

where κ_{SPR} is the complex wave number of the surface plasmon, with ϵ_1 and ϵ_3 denoting the dielectric function of the sample and the metal, respectively. We restrict ourselves to a single wavelength, allowing the dispersion of the constituent materials to be omitted. Of course, the analysis here can be performed for any wavelength, and by superposition could thus be extended to treat the response of the device to pulsed irradiation.

We expand r_{31} in the neighborhood of the pole (5), and we express the reflection coefficient in the form

$$r_{31} \cong \frac{\kappa_s}{\kappa - \kappa_{\text{SPR}}}. \quad (6)$$

The complex pole strength parameter κ_s is found to be

$$\kappa_s = - \frac{2\epsilon_1^2 \epsilon_3^2}{(\epsilon_1 + \epsilon_3)(\epsilon_1^2 - \epsilon_3^2)} \frac{\tilde{\omega}^2}{\kappa_{\text{SPR}}}, \quad (7)$$

which is a general expression and valid for absorbing samples (complex valued ϵ_1) as well. We demonstrate the validity of the pole expansion by comparing calculated reflectance to the exact one in a case, where the SPR sensor is in vacuum. This choice is made only for the sake of simplicity, for with it the pole strength parameter can be approximated as real for typical metals, such as Ag and Au, whose real part of the dielectric function is much larger than the

imaginary part *i.e.* $|\text{Re}\{\epsilon_3\}| \gg |\text{Im}\{\epsilon_3\}|$. Hence, the pole strength is given approximately by [16]

$$\kappa_s = -4(\text{Re}\{\kappa_{\text{SPR}}\} - \tilde{\omega}). \quad (8)$$

To obtain the SPR reflectance R_{51} we consider the squared modulus of complex reflectivity \tilde{r}_{51} . By a tilde we denote an effective Fresnel coefficient connecting the two indicated media, where there may be any number of layers of other media in between. For example, referring to Fig. 1a,

$$\tilde{r}_{51} = r_{53} + \frac{t_{53}r_{31}t_{35}\exp(2iw_3d)}{1 - r_{31}r_{35}\exp(2iw_3d)} = \frac{r_{53} + r_{31}\exp(2iw_3d)}{1 - r_{31}r_{35}\exp(2iw_3d)}, \quad (9)$$

where we have used the Fresnel coefficient identity (4). Equation (9) gives us directly the observed reflectance from the SPR set-up (Fig. 1a); the pole approximation results from using the approximation (6) rather than the exact expression for r_{31} .

One advantage of the pole expansion analysis is that analytic expressions (albeit approximate) for the reflectivity \tilde{r}_{51} are easily obtained and physically interpreted; we will see another advantage in Section 2.2. We write reflection coefficient $r_{53} = -r_{35} = A\exp(-i\phi)$, where both A and ϕ are real. Thus we are in the total-internal-reflection regime, and for highly reflecting metals $A \approx 1$ and $|r_{53}| = |r_{35}| = 1$. The phase of this coefficient in this approximation is obtained from the expression

$$\phi = 2 \tan^{-1} \left(\frac{\text{Im}\{w_3\}\epsilon_5}{\text{Re}\{w_5\}\text{Re}\{\epsilon_3\}} \right) \quad (10)$$

with both w_3 and w_5 calculated at the pole with $\kappa = \kappa_{\text{SPR}}$. It is convenient to separate the real and imaginary parts of the complex pole κ_{SPR} and express r_{31} as follows:

$$r_{31} = \frac{\kappa_s}{\kappa - (\kappa_m + i\gamma)} \quad \text{with} \quad \kappa_m + i\gamma = \kappa_{\text{SPR}}. \quad (11)$$

Then SPR reflectance $R_{51} = |\tilde{r}_{51}|^2$ is found, inserting these expressions into Eq. (9), to be given by

$$\begin{aligned} R_{51} &= \left| \frac{\exp(-i\phi) + \beta r_{31}}{1 + \beta r_{31} \exp(-i\phi)} \right|^2 \\ &= 1 - \frac{4\beta \text{Im}\{r_{31}\} \sin \phi}{1 + \beta^2 |r_{31}|^2 + 2\beta (\cos \phi \text{Re}\{r_{31}\} + \sin \phi \text{Im}\{r_{31}\})}, \\ &= 1 - \frac{4\beta \gamma \kappa_s \sin \phi}{(\kappa - \kappa_m + \beta \kappa_s \cos \phi)^2 + (\gamma + \beta \kappa_s \sin \phi)^2}, \end{aligned} \quad (12)$$

where we approximate the Fabry-Perot phase factor of Eq. (9) in the vicinity of the pole by $\beta = \exp(2iw_3d) \approx \exp(-2\tilde{\omega}\sqrt{1 - \epsilon_3}d)$. Here we consider incident wavelength $\lambda = 1.532 \mu\text{m}$ to have a reasonable comparison between the conventional SPR sensor and our suggested PS sensor.

We end this subsection by calculating the reflectance from a standard SPR device with a silver film (refractive index $n_2 = 0.462 + 9.20i$ [18], thickness $d = 40 \text{ nm}$) on top of the rutile prism (refractive index $n_3 = 2.55$). The comparison between the exact SPR reflectance (solid line) and the SPR reflectance obtained from the pole expansion (dashed line) is presented in the Fig. 2. The exact curve is calculated from Eq. (9) and the pole expansion curve from Eq. (12). We observe a good fit close to the pole, near the minimum of the reflectance. The discrepancy between the exact calculation and the pole analysis arises largely, because β varies over the angular spread of the surface plasmon dip, while in the pole analysis it is treated as a constant.

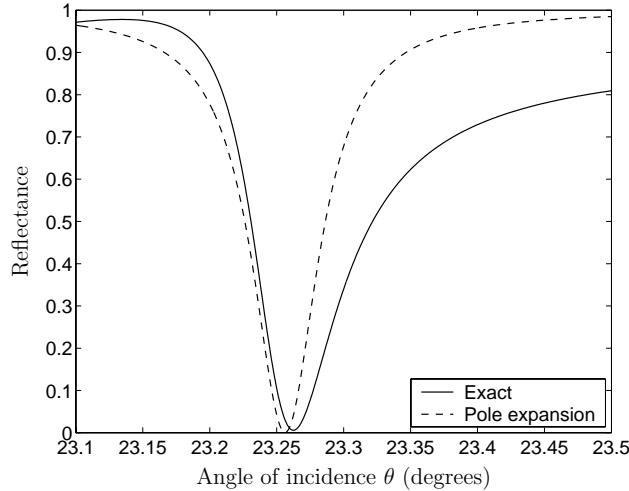


Fig. 2. Comparison of the reflectivity dip for SPR sensor with the optical constants given in the text. Dashed line, pole approximation; solid line, exact calculation.

While this pole expansion is of course not necessary for analyzing the SPR sensor, which even with the addition of the adsorptive layer can always be modelled in a straight-forward way by transfer matrices, it is convenient for identifying the parameters κ_m , κ_s , β , and ϕ on which the performance of the device depends. It also leads to a natural comparison of the standard SPR sensors with the PS sensor to which we now turn.

2.2. Pole expansion of the reflectance R_{51} from the PS sensor

Porous silicon structures contain air pores perpendicular to the interfaces and these structures display birefringence. We denote the different dielectric tensor elements $\epsilon_{xx} = \epsilon_{yy} = \epsilon^{\parallel}$ and $\epsilon_{zz} = \epsilon^{\perp}$, where z is the direction normal to the interfaces. Here we assume the air pores to be small compared to the wavelength of light, as they are for many fabrication protocols [11], allowing us to treat the porous silicon as an effective medium. We consider s-polarized light, which experiences only ϵ^{\parallel} ; the analysis of p-polarized light, which involves both ϵ^{\parallel} and ϵ^{\perp} , is left to a future communication.

In our proposed PS sensor, light is coupled through the silicon substrate using a high-index prism to the porous silicon layers. A waveguide mode is excited evanescently through the low-index (high porosity) coupling layer to the high-index (low porosity) resonator layer. For the evanescent fields in the regions 1 and 3 we have $n_2\tilde{\omega} > \kappa > n_1\tilde{\omega}, n_3\tilde{\omega}$, and the poles of r_{31} are associated with the usual dispersion relation for the waveguide modes [19]

$$\tan(hd) = \frac{q+p}{h(1-qp/h^2)}, \quad (13)$$

where we denote $w_1 = iq$, $w_2 = h$, and $w_3 = ip$ with $q, h, p \in \mathbb{R}$, and where d is the thickness of the waveguide layer. Equation (13) is an implicit equation for κ as a function of the resonator layer thickness d ; the waveguide modes, labelled by κ_m , are the solutions of this equation. These wave numbers are real, as we assume silicon to be non-absorbing at the frequency of interest.

The pole expansion of the reflectivity \tilde{r}_{31} from the waveguide layer in Fig. 1b is given by Eq.

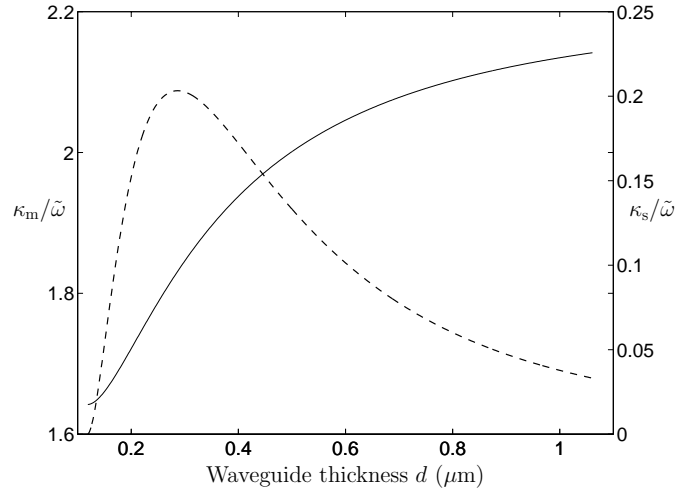


Fig. 3. Dispersion curve $\kappa_m/\tilde{\omega}$ (solid line) and pole strength parameter $\kappa_s/\tilde{\omega}$ (dashed line) as a function of the waveguide thickness d . For both curves $\lambda = 1.532 \mu\text{m}$, $n_1 = 1.00$, $n_2 = 2.213$, and $n_3 = 1.642$. The pole has a maximum value when $d = 287.2 \text{ nm}$, which we choose to be the thickness of the resonator layer.

(9) with the replacements $3 \rightarrow 2$ and $5 \rightarrow 3$. The pole expansion takes the form

$$\tilde{r}_{31} \cong \frac{\kappa_s}{\kappa - \kappa_m}, \quad (14)$$

where the real valued pole strength parameter κ_s is found, after some tedious algebra, to be [17]

$$\kappa_s = \frac{2p_m h_m^2}{\kappa_m \tilde{\omega}^2} \frac{1}{\epsilon_1 - \epsilon_2} \frac{q_m p_m}{q_m + p_m + q_m p_m d}, \quad (15)$$

and all parameters with index m are calculated at the pole, using the value $\kappa = \kappa_m$. As an example, we consider the same incident wavelength of $\lambda = 1.532 \mu\text{m}$ as in SPR calculations; the refractive index of doped silicon is practically the same as for undoped silicon ($n_{\text{Si}} = 3.4784$ [18]), and absorption is not taken into account in the thin porous silicon layers considered here. The porosities of the resonator and coupling layers are chosen here to be 50% and 75%, respectively. From a Maxwell Garnett (MG) effective medium theory for cylinders [12] we then obtain the following indices for the resonator and coupling layers: $n_{\text{Res}}^{\parallel} = 2.213$, $n_{\text{Res}}^{\perp} = 2.559$ and $n_{\text{Cpl}}^{\parallel} = 1.642$, and $n_{\text{Cpl}}^{\perp} = 1.943$. In Fig. 3 we present the numerical solution of the dispersion relation for κ_m and pole strength parameter κ_s as a function of the waveguide thickness d . We observe a cutoff value in the thickness of the waveguide that can support waveguide modes in the asymmetric waveguide, as expected [19]. The pole strength shown in Fig. 3 displays a maximum at $d = 287.2 \text{ nm}$.

So far \tilde{r}_{31} has been considered as purely real, and all the incident light in the geometry of Fig. 1b would be reflected, since no energy is dissipated in the structure and in the evanescent region of interest none could propagate into medium 1. However, there exists scattering losses from the pores in the PS layers. As a first approximation we neglect the scattering losses in the coupling layer, since at resonance the electric field is concentrated in the waveguide layer. We introduce a phenomenological scattering parameter γ to take into account losses in the resonator

layer, and adjust the pole expansion Eq. (14),

$$\tilde{r}'_{31} \cong \frac{\kappa_s}{\kappa - (\kappa_m + i\gamma)}, \quad (16)$$

where the value of γ is to be determined experimentally. Thus the pole κ_m is now shifted to a complex wave number $\kappa_m + i\gamma$ in analogy to the pole κ_{SPR} in the SPR pole expansion. This shows another strength of the pole analysis, as the approach gives a simple phenomenological treatment of scattering. Of course, one could phenomenologically include scattering losses using the transfer-matrix approach by adding an imaginary part to the dielectric function of the waveguide layer. However, the pole expansion gives us analytical expressions for the optimization of the structure. As well, γ can be set immediately from the experimentally determined waveguide loss; for porous silicon structures such as those we consider here that loss can range from 1–90 dB/cm [20].

The observed reflectance R_{51} from the PS sensor can now be calculated from the usual combinations of Fresnel coefficients that appear in thin film optics. For the ideal structure shown in Fig. 1b, but taking into account the scattering described above, we would have $R_{51} = |\tilde{r}_{51}|^2$, where

$$\tilde{r}_{51} = r_{54} + \frac{t_{54}\tilde{r}_{41}t_{45}\exp(i2w_4s)}{1 - r_{45}\tilde{r}_{41}\exp(i2w_4s)} \quad (17)$$

with

$$\tilde{r}_{41} = \frac{r_{43} + \tilde{r}'_{31}\exp(i2w_3D)}{1 - r_{34}\tilde{r}'_{31}\exp(i2w_3D)}. \quad (18)$$

However, the silicon substrate can be quite thick, and fluctuations of its thickness over the beam size typically wash out the Fabry-Perot oscillations described by the factors $\exp(i2w_4s)$ in (17). Hence we can set the denominator in the second term of (17) equal to unity and neglect the interference between the two terms. This yields

$$R_{51} = |r_{54}|^2 + |1 - r_{54}^2|^2 |\exp(i2w_4s)|^2 R_{41}, \quad (19)$$

where $R_{41} = |\tilde{r}_{41}|^2$. The absorption in the silicon substrate (thickness $s = 500 \mu\text{m}$) is estimated from the doping level, which is less than 10^{18} B atoms per cm^3 . Using Fig. 2 from Schmid [13], we estimate a value $\alpha = 1 \text{ cm}^{-1}$ for the absorption, which corresponds to a value 1.22×10^{-5} for the extinction coefficient in the doped silicon substrate.

Since at angles of incidence of interest the fields are propagating in medium 4 and evanescent in region 3, we have $r_{43} = -r_{34} = \exp(-i\phi)$, and we approximate ϕ by its value at the waveguide resonance κ_m ,

$$\phi = 2 \tan^{-1} \left(\frac{\kappa_m^2 - \tilde{\omega}^2 \epsilon_3}{\tilde{\omega}^2 \epsilon_4 - \kappa_m^2} \right)^{1/2}. \quad (20)$$

We also approximate the purely imaginary w_3 by its value at the resonance, $w_3 = ip_m$, and put $\exp(i2w_3D) \approx \beta = \exp(-2p_mD)$. Then

$$R_{41} = \left| \frac{\exp(-i\phi) + \beta \tilde{r}'_{31}}{1 + \beta \tilde{r}'_{31} \exp(-i\phi)} \right|^2. \quad (21)$$

Equation (21) is analogous to the expansion (12) used for the SPR reflectance. Hence the expansion of the reflectance R_{41} is exactly the same as the first one of Eqs. (12), except that we have \tilde{r}'_{31} instead of r_{31} . Using (19), we then find

$$R_{51} = |r_{54}|^2 + |1 - r_{54}^2|^2 |\exp(i2w_4s)|^2 \left[1 - \frac{4\beta\gamma\kappa_s \sin \phi}{(\kappa - \kappa_m + \beta\kappa_s \cos \phi)^2 + (\gamma + \beta\kappa_s \sin \phi)^2} \right], \quad (22)$$

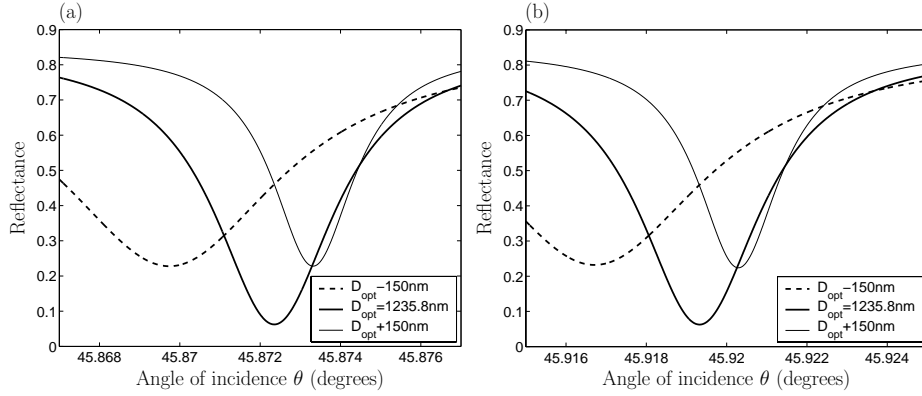


Fig. 4. Reflectance from the proposed PS sensor as a function of the angle of incidence (a) without nanoparticles and (b) with nanoparticles filling 1% of the volume of the pores. The three curves correspond to different coupling layer thicknesses with overcoupled (dashed line), optimal coupling (bold solid line), and undercoupled (thin solid line) case.

cf. Eq. (12). The minimum reflectivity is obtained when $\kappa = \kappa_m - \beta \kappa_s \cos \phi$, which corresponds to the critical angle of incidence θ_{crit} . In silicon substrate ($\kappa = n_4 \tilde{\omega} \sin \theta$) this angle is given by

$$\theta_{\text{crit}} = \sin^{-1} \left(\frac{\kappa_m - \beta \kappa_s \cos \phi}{n_4 \tilde{\omega}} \right) \quad (23)$$

and the corresponding critical angle of incidence in the rutile prism is calculated from Snell's law. At this particular angle the minimum reflectivity is

$$[R_{41}]_{\text{min}} = \left[\frac{\gamma - \beta \kappa_s \sin \phi}{\gamma + \beta \kappa_s \sin \phi} \right]^2, \quad (24)$$

which goes to zero if we set $\gamma = \beta \kappa_s \sin \phi$. This condition corresponds to a situation where all the incident light is coupled into a waveguide mode and absorbed by the scattering losses. We obtain the optimal coupler thickness D_{opt} , using the definition of $\beta = \exp(-2p_m D)$, in the form

$$D_{\text{opt}} = -\frac{1}{2p_m} \ln \left[\frac{\gamma}{\kappa_s \sin \phi} \right]. \quad (25)$$

The reflectance from the PS sensor goes to minimum value at the critical angle with this particular coupler thickness, and we can optimize our structure by choosing this value of D . The thickness of the resonator layer can be chosen arbitrarily, but the best sensitivity of the sensor is obtained where the pole strength is largest. The minimum value and the width of the reflectance dip is larger for smaller coupler thicknesses as the light is coupled too efficiently back to the silicon substrate. On the other hand, the excitation of the waveguide mode is reduced if the coupling layer is thicker than the optimal value, leading to an increase in the minimum value of the reflectance.

3. Numerical comparison between PS and SPR sensors

We demonstrate the performance of our proposed sensor by a sample calculation. We imagine a rutile prism ($n=2.55$) placed below the silicon substrate to facilitate optical coupling into the waveguide resonance. We use the pole expansion, developed in the previous section, which is

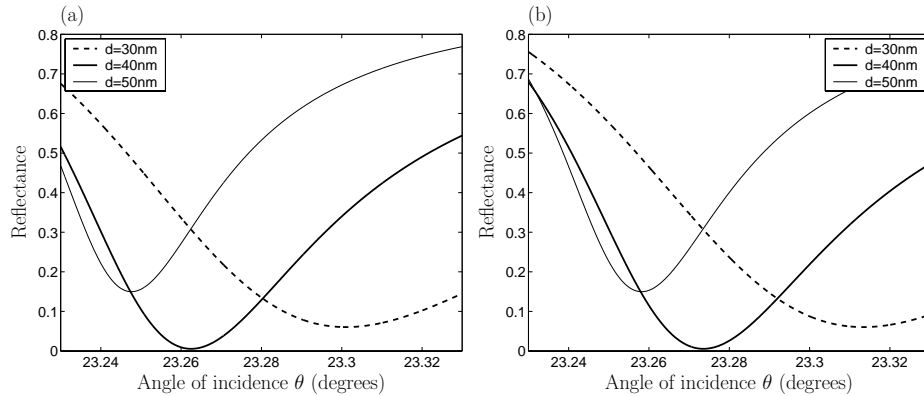


Fig. 5. Reflectance from the conventional SPR sensor as a function of the angle of incidence (a) in vacuum and (b) with 1 nm thick polymer film on top of the metal film. The three curves correspond to different metal thicknesses of overcoupled (dashed line), optimal coupling (bold solid line), and undercoupled (thin solid line) case. The peaks in SPR are much broader than the peaks with our proposed PS sensor. Note that here the x -axis spans an angle 10 times larger than in the Fig. 4 for the PS sensor.

limited to angles of incidence for which fields are evanescent in both the coupler and air but not in the resonator; we include these scattering losses by adding the appropriate imaginary part γ to the resonance wave number associated with the waveguide mode. We take $\gamma = 115.13 \text{ m}^{-1}$, corresponding to a waveguide loss of 10 dB/cm. This is well within the range of losses observed for structures such as these [20]. We take a resonator layer thickness to be $d = 287.2 \text{ nm}$, which corresponds to the maximum value of the pole strength curve presented in Fig. 3. The optimal thickness of the coupling layer is found to be $D = 1235.8 \text{ nm}$ from Eq. (25). From an experimental point of view the etching of 290 nm low-porosity layer on top of 1.24 micron high porosity layer on silicon substrate is straightforward [11]. Furthermore, the device operation is not dramatically sensitive to the thickness of the coupling layer, as we see from the results displayed in Fig. 4. For larger values of D (thin solid lines) the system is undercoupled and we obtain smaller reflectivity dips, while for smaller D (dashed lines) the dips become broader as the light is coupled too efficiently back to the reflected field.

As a simple model for a detection scenario, we consider partially filling the pores of the waveguide layer with nanoparticles of refractive index $n = 1.59$, and compare the reflectance with that of the structure before filling. Assuming that the nanoparticles fill 1% of the volume of the pores, we model the new refractive index of these pores with the Maxwell Garnett theory for spheres in air. For the resonator layer, the MG effective medium theory for cylinders [12] then yields a new $n_{\text{Res}}^{\parallel} = 2.215$. The predicted reflectances before and after filling are shown in Figs. 4a and 4b, respectively. For the air pores we obtain a narrow reflectance dip at an angle of incidence of 45.872° , while for pores partially filled with nanoparticles the corresponding resonance angle is 45.919° , yielding a shift of $\Delta\theta = 0.047^\circ$. This shift is well in the detection range as the half-width of the dip, which is approximately 0.004° with optimized coupler thickness.

We compare our proposed PS sensor with a standard SPR device (shown in Fig. 1 a) by considering silver metal, with refractive index $n_{\text{Ag}} = 0.462 + 9.20i$ at $\lambda = 1.532 \mu\text{m}$ [18], on top of a rutile prism. We observe the best sensitivity of the device operation by taking a metal thickness of $d = 40 \text{ nm}$, as shown in Fig. 5a. For larger thicknesses the reflection minimum increases as the excitation of surface plasmon is reduced due to absorption of the metal film; for smaller thicknesses the surface plasmon is coupled too strongly back to the reflected field

and the reflectance dips become broader as seen from Figs. 5a and b.

In the SPR sensor the target material to be detected is taken to be on top of the metal film. In our PS calculation the pore volume in a surface area A of the detector was $(0.5)(287\text{nm})A$, of which 1% was filled with nanoparticles with $n = 1.59$. The same amount of material per area A here, spread uniformly over the surface of the SPR sensor, would result in an overlayer of thickness $(0.01)(0.5)(287\text{nm})=1.44\text{nm}$. We calculate the optical response here using the transfer matrices, without applying a pole approximation. But we note that a calculation with the pole approximation would lead to essentially the same shifts and widths we find below [21].

We see from Fig. 5a that without the overlayer the SPR resonance angle of incidence is 23.263° , while with the overlayer the resonance angle is 23.274° . This yields a shift of $\Delta\theta = 0.011^\circ$ with a half-width of the SPR resonance dip approximately 0.06° for the optimized metal thickness. Furthermore, this shift is smaller than that predicted shift for the PS sensor, and can be associated with the fact that the target material is exposed only to evanescent fields in the SPR sensor; in the PS sensor, on the other hand, the target material exists within the volume of the waveguide and is exposed to the full field of the waveguide mode. Perhaps more importantly, the dips are significantly broader in the SPR sensor than predicted for the PS sensor. This arises because the scattering loss of the PS sensor waveguide mode, even at 10 dB/cm, is less than the absorption loss of typical surface plasmons; the γ for the SPR sensor that follows from (11) corresponds to 214 dB/cm. Note that any surface roughness or defects near the metal surface would only increase the SPR resonance width.

A reasonable figure of merit with which to compare the devices would be the shift in the position of the resonance dip divided by the width of that dip. For our example, that figure of merit is approximately 0.20 for the SPR sensor, and approximately 12 for the PS sensor. Hence the presence of the target material would clearly be much easier to detect with our proposed PS sensor. Finally, we note that the operation of the SPR sensor is qualitatively the same if considered at visible wavelengths. We will turn to a discussion of PS sensors in that region of the spectrum in a future communication.

4. Conclusions

Our calculations show that the proposed PS sensor should show a sensitivity to target materials greater than conventional SPR sensors. The target material can be placed inside the resonator, precisely where the excited resonance fields are the strongest, and the scattering losses in PS structures are much less than the absorption losses in surface plasmons, leading to narrower dips in the PS sensor than in an SPR device. The continuing improvement of the quality of PS films promises even better possible sensitivity in the future. Furthermore, the PS device should be easy and inexpensive to fabricate.

Another advantage of the structure is the possibility of choosing a pore size in the resonator layer that will only accept target material of interest. Work underway includes experimental studies of these devices, both in the infrared and visible regime, and further theoretical design studies to optimize performance.

Acknowledgments

Author JJS wishes to thank the Academy of Finland (grant no. 204925 & 204109) for financial support. This work was partially supported by the Natural Sciences and Engineering Research Council of Canada.

*Permanent address, Department of Physics, University of Joensuu, P.O. Box 111, FI-80101 Joensuu, Finland.